Properties of Poly(ethylene oxide)−Poly(butylene oxide) Diblock Copolymers at the Interface between Hydrophobic Surfaces and Water

Karin Schillén,* Per M. Claesson, and Martin Malmsten

Laboratory for Chemical Surface Science, Department of Chemistry, Physical Chemistry, Royal Institute of Technology, S-100 44 Stockholm, Sweden, and Institute for Surface Chemistry, P.O. Box 5607, S-114 86 Stockholm, Sweden

Per Linse

Physical Chemistry 1, Center for Chemistry and Chemical Engineering, Lund University, P.O. Box 124, S-221 00 Lund, Sweden

Colin Booth

Manchester Polymer Centre, Departments of Chemistry and Pharmacy, University of Manchester, Manchester M13 9PL, U.K.

Received: October 17, 1996; In Final Form: January 24, 1997[⊗]

The interactions between molecules of a low molecular weight diblock copolymer of poly(ethylene oxide) (E) and poly(butylene oxide) (B), B_8E_{41}, at hydrophobic surfaces were investigated experimentally by using two surface force techniques and ellipsometry. Extended mean-field theory was employed to describe the adsorption of EB diblock copolymers at planar surfaces as well as the forces between surfaces with adsorbed diblock copolymers. It is the hydrophobic poly(butylene oxide) block that anchors the diblock copolymer at the hydrophobic surface with the water-soluble poly(ethylene oxide) block protruding in the aqueous solution in a "brushlike" or at least stretched structure. The adsorption kinetics demonstrate that two adsorption regimes exist, one which is transport-limited and the other at higher adsorption where a slower branch due to crowding effects at the surface exists. Only monotonic repulsive steric forces between the diblock copolymer-coated surfaces were observed in the surface force measurements. The range of the steric repulsion increased with increasing bulk copolymer concentration, whereas the concentration of an inert salt (KBr, up to 0.1 M) did not influence the measured steric interaction. Upon dilution the block copolymer slowly dissolved, which resulted in a less long-range steric force, and under a high force the layers were squeezed out from between the surfaces. The adsorbed layer thickness obtained in the experiments varied with solution volume-to-surface area ratio. This is interpreted as being caused by the polydispersity of the diblock copolymer. The interaction parameters entering the mean-field model were fitted to reproduce adsorption isotherms of the diblock copolymer and of two triblock copolymers of different architectures. Calculations were performed for mondisperse and polydisperse diblock copolymers. The agreement between theory and experiement was improved when the molecular polydispersity ($M_m/M_n = 1.1$) of the sample was taken into account. In particular, polydispersity led to predicted adsorption isotherms that are more of the high affinity type and more sensitive to low volume-to-surface area ratio and to the interaction between surfaces starting at a longer separation. Among the polymer components, it is those with the largest B block that adsorb preferentially, which leads to an increased amount adsorbed and forces the E chains to adopt more extended conformations.

1. Introduction

Block copolymers have lately been extensively investigated primarily because of their usefulness in several industrial applications, such as steric stabilizers in paints, pharmaceutical, and food formulations, solubilizers of hydrophobic substances, gelling agents, etc. Much of the work regarding the aqueous solution properties and phase behavior of block copolymers has focused on poly(ethylene oxide)−poly(propylene oxide) (EP) block copolymers. These systems have been studied for many years using various experimental techniques. Reasons for this are that EP block copolymers (a) were among the first to be commercially available, (b) have a low toxity, and (c) have an interesting physicochemical behavior (e.g. a reversed temperature micellization and gelation). A comprehensive knowledge about the micellization[1] and the adsorption at solid and fluid interfaces[2] has been achieved from the different experiments. Similarly, tethered polymers have received great attention from a theoretical point of view and their properties have been modeled with various theories with different degrees of sophistication.[2−4] From both a fundamental and practical point of view, however, EP block copolymers leave much to be desired, since (a) they are polydisperse and (b) there is not a clear segregation between the E and the P blocks. To remedy this, interest has emerged around other aqueous block copolymer systems. One new such class of block copolymers is poly(ethylene oxide)−poly(butylene oxide) (EB) block copolymers.

EB block copolymers in aqueous solution have been investigated regarding micellization and gelation in several studies.[5−8] It has been found that the critical micelle concentration (cmc) is lower for diblock copolymers than for triblock copolymers. Additionally, the association number of the diblock copolymers is seen to be generally higher than those of the triblock

[⊗] Abstract published in *Advance ACS Abstracts,* March 15, 1997.

S1089-5647(96)03193-8 CCC: $14.00

copolymers of comparable B block length. This was concluded in an investigation concerning the effect of chain structure on micellization, where also a comparison was made among EB, EP, and E-alkyl block copolymers.[9] It was found that in diblock copolymers with equal E block length, the effect of a butylene oxide unit on the cmc is approximately the same as that of an alkyl unit. The study also showed that there is a more pronounced segregation between the different blocks in the EBE triblock copolymers compared to the EPE triblock copolymers because of the fact that poly(butylene oxide) is more hydrophobic than poly(propylene oxide).

Up to now, little work has been aimed at investigating the surface properties of block copolymers composed of poly(ethylene oxide) and poly(butylene oxide). The study presented here is one exception. In this study experimental data from two complementary techniques have been combined with results from theoretical modeling in order to obtain further insight about the adsorption of the diblock copolymer, B_8E_{41}. Ellipsometry has been used to measure the adsorbed amount, and two types of surface force apparatuses have been used to obtain the interaction between surfaces with adsorbed diblock copolymers. The theoretical model calculations are based on a mean-field lattice theory developed by Scheutjens and Fleer.[10,11] The diblock copolymer selected is composed of butylene oxide and ethylene oxide with an average composition of B_8E_{41}. Despite its low polydispersity ($M_m/M_n = 1.1$), the chemical difference between butylene oxide and ethylene oxide is sufficient to give rise to pronounced polydispersity effects: (i) slow adsorption, (ii) larger adsorption at low polymer concentrations than expected for a monodisperse system, and (iii) force curves dependent on the volume-to-surface area ratio. Items ii and iii are supported by the model calculations, which also provide detailed information on the volume fraction profiles and the preferential adsorption of the copolymer components.

The paper is organized as follows. In section 2 some of the mean-field lattice theory for heterogeneous systems, which is applicable to the situation of this study, is reviewed. In particular, the polydispersity model and how the interaction parameters used have been obtained are described. The following section reports on the materials used, experimental setups, and procedures applied. The results of the ellipsometry and surface force measurements, as well as the model calculations, are given in section 4. Section 5 deals with discussions on the adsorption isotherms, structure of the adsorbed layer, and the surface force profiles.

2. Model Calculations

2.1. Theory. The Flory−Huggins lattice theory of homogeneous solutions[12] has been extended by Scheutjens and Fleer[10,11] to describe the adsorption of flexible polymers at surfaces. Since then, the heterogeneous lattice theory has been further extended in several directions and applied to a number of different cases.[2] Here, only a brief account of the theory adapted to block copolymer adsorption at planar surfaces and forces between surfaces with polymers adsorbed will be given. For a more detailed description of the lattice theory and nomenclature used, see, for example, refs 10, 11, 13, and 14.

In the application used here, the polymer solution in the vicinity of an impenetrable surface is divided into layers parallel to the planar surface as illustrated in Figure 1. The layers available to the polymer or solvent molecules are numbered $i = 1, 2, ..., M$ starting from the layer adjacent to the surface. The thickness of the layers corresponds to the size of the polymer segment. Within each layer, the Bragg−Williams approximation of random mixing is applied, and thus, all lattice sites in a layer are equivalent. A hexagonal lattice has been chosen, and thus, the number of nearest-neighbor sites, z, is 12. The lattice is completely filled by a mixture of two components (solvent and polymer). There are n_x molecules of component x, and each molecule consists of r_x segments (1 or $r_{polymer}$). There are two types of polymer segments: E and B. The solvent or polymer segments are referred to as species.

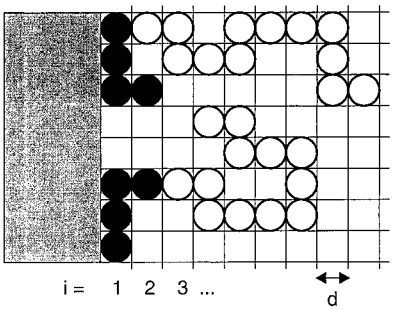

Figure 1. Illustration of a semi-infinite lattice bounded by a solid surface (shaded area) at which diblock copolymers (open and filled circles) are adsorbed and solvent (unfilled lattice cells). The layer numbering perpendicular to the surface and the lattice cell size d are also indicated.

The presence of a surface introduces a unique direction (the normal) in the system. The complete directional degeneracy of the segment spatial distribution in the homogeneous system is thus lifted, and various conformations of the polymer chains can be distinguished according to the different ordering of their segments with respect to the layer numbers. Formally, a conformation c of component x is defined as a sequence of layer numbers, where the sth number is the layer number where the sth segment of a chain of component x in conformation c resides. With this definition, and neglecting at first self-exclusion, the degeneration of a conformation c of component x becomes $\exp[(r_x - 1)\ln z + \ln \omega_{xc}]$. The factor ω_{xc} is a product of the number of sites in the layer, where the first segment is located, and λ_{ij} factors, one for each segment except the first, which gives the probability of arranging the segments according to conformation c. λ_{ij} denotes the fraction of nearest-neighbor sites in layer j viewed from a site in layer i.

The derivation of the segment distribution starts from the partition function of the model system. After replacement of the partition function with its largest term, the (Helmholtz) free energy of the system relative to the reference state (designated with *) of separated amorphous components may be expressed as

$$\beta(A - A^*) = -\ln \frac{\Omega}{\Omega^*} + \beta(U - U^*) \qquad (1)$$

where $\beta = (kT)^{-1}$, k being the Boltzmann constant and T the absolute temperature. The first term on the right-hand side of eq 1 denotes the mixing entropy and the second one the mixing energy.

When the self-exclusion on a mean-field level is taken into account and the contributions from all conformations of all the components are included, the total conformational degeneration relative to the amorphous reference state, constituting the mixing entropy of the system, is given simply by

$$\ln \frac{\Omega}{\Omega^*} = -\sum_x \sum_c n_{xc} \ln \frac{n_{xc} r_x}{\omega_{xc}} \qquad (2)$$

where n_{xc} denotes the number of chains of component x in conformation c.

Within the mean-field approximation, the interaction energy is given by

$$\beta U = \frac{1}{2} L \sum_{i=0}^{M} \sum_{\mathrm{A}}^{\mathrm{s}} \sum_{\mathrm{A}'}^{\mathrm{s}} \phi_{Ai} \chi_{\mathrm{AA}'} \langle \phi_{\mathrm{A}'i} \rangle \tag{3}$$

where L is the number of lattice sites in a layer and $\langle ... \rangle$ denotes an average over the actual and adjacent layers according to $\langle x_i \rangle = \lambda_{i,i-1} x_{i-1} + \lambda_i x_i + \lambda_{i,i+1} x_{i+1}$. The notation $\sum^{\mathrm{s}}$ implies that the sum includes the surface species as well. In eq 3, $\chi_{\mathrm{AA}'}$ denotes the Flory−Huggins interaction parameter[12] traditionally defined as $\chi_{\mathrm{AA}'} = \beta z[\epsilon_{\mathrm{AA}'} - (\epsilon_{\mathrm{AA}} + \epsilon_{\mathrm{A}'\mathrm{A}'})/2]$, where $\epsilon_{\mathrm{AA}'}$ is the interaction energy on a site volume basis between species A and A′. In the case of the block copolymer, the reference interaction energy U^* in eq 3 is nonzero (see, for example, eq A.5.2. of ref 14).

The expression for the segment distribution (E and B segments and solvent) can now be obtained. Minimization of the free energy with respect to $\{n_{xc}\}$ and the packing constraint results in an expression for the layer-dependent species potential $u_{\mathrm{A}i}$, which denotes the relative free energy of an unconnected segment of type A being located in a layer i. The species potential can be divided into two parts, one species independent, u_i', and the other dependent on the species, $u_{\mathrm{A}i}^{\mathrm{int}}$, according to

$$u_{Ai} = u_i' + u_{\mathrm{A}i}^{\mathrm{int}} \tag{4}$$

If the species potentials are defined with respect to the bulk solution, i.e., if $u_{\mathrm{A}}^{\mathrm{b}} = 0$, then the two terms are given by

$$\beta u_i' \equiv \alpha_i + \sum_x \frac{\phi_x^{\mathrm{b}}}{r_x} + \frac{1}{2} \sum_{\mathrm{A}'} \sum_{\mathrm{A}''} \phi_{\mathrm{A}}^{\mathrm{b}} \chi_{\mathrm{A}'\mathrm{A}''} \phi_{\mathrm{A}''}^{\mathrm{b}}$$

$$\beta u_{\mathrm{A}i}^{\mathrm{int}} \equiv \sum_{\mathrm{A}'}^{\mathrm{s}} \chi_{\mathrm{AA}'} (\langle \phi_{\mathrm{A}'i} \rangle - \phi_{\mathrm{A}'}^{\mathrm{b}}) \tag{5}$$

The species-independent potential u_i', related to the lateral pressure in a continuous model, ensures that by a suitable choice of α_i the space is completely filled at layer i. In bulk, u' becomes zero. The species-dependent term $u_{\mathrm{A}i}^{\mathrm{int}}$ consists of the mixing energy for species A in layer i being diminished by the mixing energy for species A in bulk. At distances far from the surface, $\phi_{\mathrm{A}i}$ approaches $\phi_{\mathrm{A}}^{\mathrm{b}}$, and hence, $u_{\mathrm{A}i}^{\mathrm{int}}$ becomes zero.

The second aspect of determining the segment distribution is to take into account the chain connectivity. If only monomers are present, the volume fraction $\phi_{\mathrm{A}i}$ of monomer A in layer i is related only to the bulk volume fraction $\phi_{\mathrm{A}}^{\mathrm{b}}$ according to

$$\phi_{\mathrm{A}i} = G_{\mathrm{A}i} \phi_{\mathrm{A}}^{\mathrm{b}} \tag{6}$$

where the weighting factor $G_{\mathrm{A}i}$ for species A in layer i is given by

$$G_{\mathrm{A}i} = \exp(-\beta u_{\mathrm{A}i}) \tag{7}$$

since the species potentials were defined to be zero in bulk. The matter becomes more complex for polymers. However, by use of a matrix method, the *segment* distribution as expressed in terms of n_{xsi}, the number of sites in layer i occupied by segments of rank s belonging to component x, is given by

$$n_{xsi} = C_x \{\Delta_i^T \cdot [\prod_{s'=r_x}^{s+1} (\mathbf{W}^{t(x,s')})^T] \cdot \mathbf{s}\} \{\Delta_i^T \cdot [\prod_{s'=2}^{s} \mathbf{W}^{t(x,s')}] \cdot \mathbf{p}(x,1)\} \tag{8}$$

where C_x is a normalization factor (related to the amount of or to the bulk volume fraction of component x), $\mathbf{W}^{t(x,s)}$ a tridiagonal matrix comprising elements that contain factors describing the lattice topology and weighting factors for the segment of rank s belonging to component x, and $\mathbf{p}(x,1)$ a vector describing the distribution of the first segment of component x in the layers, with Δ and $\mathbf{s}$ being elementary column vectors. From n_{xsi} the segment volume fractions desired are easily obtained. The *species* volume fraction $\phi_{\mathrm{A}i}$, needed in eq 8, is given by

$$\phi_{\mathrm{A}i} = \frac{1}{L_i} \sum_x \sum_{s=1}^{r_x} \delta_{\mathrm{A},t(x,s)} n_{xsi} \tag{9}$$

where the Kronecker δ only selects segments of rank s of component x if they are of type A. Thus, given the species potentials $u_{\mathrm{A}i}$, the species volume profiles $\phi_{\mathrm{A}i}$ are obtained by eqs 7−9, these equations together with eqs 4 and 5 constituting an implicit set of nonlinear equations for the segment distributions.

A central quantity in the comparison with the ellipsometry data is the excess adsorbed amount. It is evaluated according to

$$\Gamma_{\mathrm{ex}} = \sum_i (\phi_{\mathrm{polymer},i} - \phi_{\mathrm{polymer}}^{\mathrm{b}}) \tag{10}$$

where $\phi_{\mathrm{polymer}}^{\mathrm{b}}$ is the bulk polymer volume fraction. In the case where comparison is made with surface force measurements, two surfaces are located at $i = 0$ and $M + 1$, respectively. Thus, they are separated by M layers of polymer solution. The free energy associated with the surfaces in contact with the solution, i.e., the excess surface free energy of the system, becomes

$$\mathrm{A}^{\sigma} = (\mathrm{A} - \mathrm{A}^*) - \sum_x n_x (\mu_x - \mu_x^*) \tag{11}$$

where the sum extends over the components of the system that are in equilibrium with the bulk solution. Two cases will be considered, the case where full equilibrium of both the solvent and polymer is established and the case with fixed amount of polymer between the surfaces. In eq 11, $\mu_x - \mu_x^*$ denotes the difference of the chemical potential of component x in bulk and in the reference state. Finally, the measured forces from the surface force apparatus (SFA) are related via the Derjaugin approximation (eq 13) to the free energy of interaction between the two surfaces evaluated according to

$$\mathrm{A}^{\mathrm{int}}(M) = \mathrm{A}^{\sigma}(M) - \mathrm{A}^{\sigma}(\infty) \tag{12}$$

2.2. Polymer Model. The nominal composition of the diblock copolymer is B_8E_{41}. However, the effect of polymer polydispersity on the adsorption is normally of large importance. Although the synthesis procedure of the ethylene oxide−butylene oxide block copolymer leads to a relative low polydispersity, it is still of significance for the adsorption behavior. A polydisperse model has therefore been adopted where the block copolymer sample is represented by several polymer components with different composition, which closely follows the approach taken for modeling the self-association of polydisperse ethylene oxide- and propylene oxide-containing polymers.[15] Some results pertaining to a monodisperse model are also given in order to illustrate the effects and importance of polydispersity.

By assuming that the number of segments in each block is independent of each other, one obtains for a diblock copolymer a two-dimensional polydispersity. In the model calculations, two different representations of the polydispersity were exam-

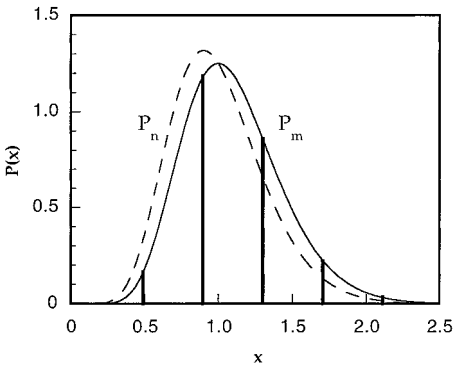

Figure 2. Number and mass distributions, $P_n(x)$ and $P_m(x)$, respectively, as a function of x for a polydispersity ratio of $M_m/M_n = 1.1$ as obtained from the Schulz−Zimm distribution function. $P(x)$ denotes the probability of $x \equiv r/\langle r\rangle_n$, where r is the number of segments in a polymer (or a block) and $\langle r\rangle_n$ the n-average number of segments of the polymer (or the block). A five-point discrete representation of $P_m(x)$ is also shown. The points were selected with constant spacing in x with $\langle x\rangle_n = 1$ and in a manner such that the same polydispersity as for the continuous representation was obtained.

ined. In the first and simplest one, the composition of the components was held constant (fixed E/B ratio), only the total *mass* being allowed to vary, whereas in the other more realistic representation, the number of segments in each block was varied independently, thus taking into account a *mass and composition* polydispersity.

All polydispersity calculations have been made by assuming a Schulz−Zimm distribution. This distribution is normally expressed using two parameters related collectively to the average and the width of the distribution.[16] In the present case, it is more convenient to consider the distribution of the reduced number of segments, $x \equiv r/\langle r\rangle_n$, where r is the number of segments and $\langle r\rangle_n$ the n-averaged number of segments. The fraction of polymers having between r and $r + dr$ segments, $P_n(r)\,dr$, and the fraction of polymer segments that are in polymers having between r and $r + dr$ segments, $P_m(r)\,dr$, become $P_n(x)\,dx$ and $P_m(x)\,dx$, respectively, where $P_n(x) = k^k x^{k-1} \exp(-kx)/\Gamma(k)$ and $P_m(x) = xP_n(x)$ using the normalization expressions $\int_0^\infty P_n(x)\,dx = 1$ and $\int_0^\infty P_m(x)\,dx = 1$ and using $\langle x\rangle_n = 1$. $\Gamma(k)$ denotes the gamma function of k. The parameter k describes the width of the distribution, and it is related to the polydispersity ratio according to $k = [M_m/M_n - 1]^{-1}$. Thus, the smaller the k, the wider the distribution becomes.

In the discrete representation, the weights of the components representing a polydisperse polymer (or a block) were calculated according to $w_j = P_m(x_j)/\sum_{j'=1}^{N} P_m(x_{j'})$, where N_p is the number of components. The members of the set $\{x_j\}$, $j = 1, 2, ..., N_p$ were selected in increasing order such that $\langle x\rangle_n = 1$ and $x_j - x_{j-1} =$ constant, $j = 2, ..., N_p$, and that they yielded the desired polydispersity ratio M_m/M_n. The selection of $\{x_j\}$ required an iterative process.

All calculations with the polydisperse model were performed with $M_m/M_n = 1.1$ and $N_p = 5$, and Figure 2 shows the corresponding continuous number and mass distributions as well as the discrete mass distribution employed. In the case of a mass and composition polydispersity, the same N_p value and polydispersity ratio were applied to both blocks for simplicity, but there is no restriction in the model for doing so. The compositions and the mass statistical weights of the 5 components of the *mass* polydisperse representation and the 25 components of the *mass-and-composition* polydisperse representation are given in Tables 1 and 2, respectively.

To perform the calculations, the parameters of the E−solvent, B−solvent, and E−B interaction as well as of their interactions with the surface are required. These parameters were obtained

TABLE 1: Mass Weight, $w \times 10^3$, of the Five Components B_aE_b Representing the Mass Polydisperse B_8E_{41} with $M_m/M_n = 1.1$ and $N_p = 5$

a	b	w
4	20	67.0
7	37	480.6
10	53	348.3
14	70	90.9
17	87	13.3

TABLE 2: Mass Weight, $w \times 10^3$, of the 25 Components B_aE_b Representing the Mass and Composition Polydisperse B_8E_{41} with $M_m/M_n = 1.1$ and $N_p = 5$

	b				
a	20	37	53	70	87
4	4.5	32.2	23.3	6.1	0.9
7	32.2	231.0	167.4	43.7	6.4
10	23.3	167.4	121.3	31.7	4.6
14	6.1	43.7	31.7	8.3	1.2
17	0.9	6.4	4.6	1.2	0.2

TABLE 3: Species−Species Interaction Parameters $RT\chi_{AA'}$ (kJ/mol) for the Polydisperse Model of the Block Copolymers

	E	B	surface[a]
water	1.0	5	10
E		4	6
B			0

[a] The absolute scale of the surface parameters is irrelevant; only the difference between two interaction parameters is significant.

TABLE 4: Species−Species Interaction Parameters $RT\chi_{AA'}$ (kJ/mol) for the Monodisperse Model of the Block Copolymers

	E	B	surface[a]
water	1.1	6	14
E		5	8
B			0

[a] The absolute scale of the surface parameters is irrelevant; only the difference between two interaction parameters is significant.

by fitting calculated adsorption isotherms to corresponding ellipsometry data of three ethylene oxide- and butylene oxide-containing block copolymers with different architecture (EB, EBE, and BEB block sequences). In the fitting procedure we required that the relative order and size of the interaction parameters were reasonable. Two fits were performed, one with the mass polydisperse and one with the monodisperse model of the block copolymers, since the two polymer models display widely different adsorption behavior and we desire to compare the two polymer models *given* similar adsorption isotherms. (The difference in the adsorption between the mass polydisperse and the mass-and-composition polydisperse representations of the polydisperse polymer model at the polydispersity ratio selected was relatively small, and hence, all calculations involving the two polydisperse polymer representations are based on the same interaction parameters.) The parameters obtained are collected in Tables 3 and 4, and as will be shown below, they give similar adsorption isotherms. We notice that $RT\chi_{E,B} = 4$ kJ/mol corresponds to $\chi_{E,B} = 1.6$ at room temperature. This is 1 order of magnitude larger than the value extracted from scattering experiments on poly(ethylene oxide)−poly(butylene oxide) melts.[43] There are several contributions to this difference. First, it was previously demonstrated that the ethylene oxide−propylene oxide interaction depends strongly on the water content in the ternary poly(ethylene oxide)−poly(propylene oxide)−water system, and when a polymer model with internal degrees of freedom was used and fitted to the experimental phase diagrams, the deduced $\chi_{E,P}$ ranged from 0.2

(50% E and 50% P) to 0.7 (100% water).[44] With the reasonable assumption that the ethylene oxide−butylene oxide interaction is also dependent on the water content in a similar way, $\chi_{E,B}$ is expected to be 3−4 times larger in an aqueous environment than in a melt. Second, in the present case the interaction parameters are based on a butylene oxide segment corresponding to one butylene oxide unit, whereas in ref 43 the volume of a butylene oxide segment in the model was 1.9 times smaller (and equal to the volume of an ethylene oxide unit). Finally, we also notice that even when the same system is used, interaction parameters extracted by fitting to experimental data can depend considerably on the experimental technique employed. Nevertheless, the use of adsorption isotherms of several polymers with different architecture makes the fits quite unique. If only one block copolymer had been used, unreasonably linear dependence among the interaction parameters would have been obtained.

Throughout, the theoretically determined excess adsorbed amounts are presented in equivalent number of monolayers (Γ^{ex}) and the interaction free energies in reduced units per unit area ($A^{int}/(kTL)$), whereas the experimentally determined adsorbed amounts (Γ) are given in mg/m^2, and the forces, normalized by the local mean radius of curvature (F/R), are given in mN/m. Taking the reasonable lattice size $d = 0.4$ nm and a mean monomeric mass of 50 g/mol, the conversion relations between experimental and theoretical values becomes $\Gamma/(\text{mg/m}^2) = 0.52\Gamma^{ex}$ and $F/R/(\text{mN/m}) = 2\pi\cdot 26A^{int}/(kTL)$ (cf. eq 13), respectively.

3. Experimental Section

3.1. Materials. The diblock copolymer (denoted B_8E_{41}) was synthezised using sequential anionic polymerization of ethylene oxide (E) and butylene oxide (B) as described in detail previously.[7] The structural formula for the average composition is $HO[CH_2CH_2O]_{41}-[CH(CH_2CH_3)CH_2O]_8H$. It has a declared formal number-average molecular weight (M_n) of 2400 and a mass-average to number-average molecular weight ratio (M_m/M_n) of about 1.1. The poly(ethylene oxide) content is 76% of the total weight of the compound.

The water used in all experiments was purified with a Millipore Milli-Q plus 185 purification system, which includes a pretreating Milli-RO 10 plus purification system. It was further degassed under vacuum for at least 1 h. Finally, the block copolymer solutions were filtered through 0.2 μm Gelman acrodisk filters. The investigated B_8E_{41} concentrations were 10, 50, and 200 ppm (w/v).

Polished silicon slides from Okmetic, Finland were used in the preparation of the silica surfaces for the ellipsometry measurements. They were of p type (boron-doped) with a resistivity of 7−13 Ω cm. The methylated silica surfaces were prepared using trichloroethylene (pro Analysi) and (dichloro)-dimethylsilane ($Cl_2(CH_3)_2Si$) from Merck.

Brown muscovite mica, a layered aluminosilicate mineral, and the epoxy glue (Epon 1004) used in the interferometric surface force measurements was received from Mica New York Corporation and from Shell Chemicals, respectively. (Dimethyl)dioctadecylammonium bromide (DDOABr) from Eastman Kodak Corporation was used for rendering the mica surfaces hydrophobic.

The MASIF glass surfaces were hydophobized by reaction with (3,3-dimethylbutyl)dimethylchlorosilane purchased from Hüls-Petrarch.

3.2. Methods. *3.2.1. Ellipsometer.* Adsorption measurements on the diblock copolymer B_8E_{41}−water system were performed by means of null ellipsometry[17] using an automated Rudolph thin-film ellipsometer, Type 436, controlled by a personal computer. An xenon lamp filtered to 4015 Å was used as the light source. A thorough description of the experimental setup has been given previously.[18]

3.2.2. Interferometric Surface Force Apparatus. The forces acting between hydrophobized molecularly smooth mica surfaces coated by the diblock copolymer B_8E_{41} were investigated by using the surface force apparatus (SFA) of Israelachvili and Adams (Model Mark II).[19] In the SFA, the force is directly measured as a function of the absolute surface separation (i.e., force−distance profiles).

The area of each mica sheet was about 1 cm^2. They were silvered on one side, glued with the silver side down onto cylindrical silica disks, and then hydrophobized, as described below. Directly after surface modification, the disks were mounted in a crossed cylinder configuration inside the SFA.

During measurements the surface separation (D) is changed by moving the upper surface with a piezoelectric crystal device or by using a synchronous motor coupled by a differential spring system to the lower surface. D is determined with an accuracy of about 0.2 nm by using optical interferometry.[20] Owing to the silvering of the mica sheets, multiple reflection of the light will occur between their back-sides and only the wavelengths that interfere constructively will pass through the apparatus. The transmitted light is then analyzed in a spectrometer.

From measurement of the deflection of the spring supporting the lower surface, the force (F_{cc}) is determined, using the equation of Hooke, with a lower detection limit of 10^{-7} N. The spring constant was determined after each experiment. The force acting between crossed cylinder surfaces at a separation D, $F_{cc}(D)$, is related to the free energy of interaction per unit surface area between two flat surfaces, $G_f(D)$, according to the Derjaguin approximation:[21]

$$\frac{F_{cc}(D)}{R} = \frac{F_{sf}(D)}{R} = \frac{2F_{ss}(D)}{R} = 2\pi G_f(D) \qquad (13)$$

where R (∼2 cm) is the local geometric-mean radius of curvature of the undeformed surfaces. The local radius may be determined from the shape of the interference fringes. F_{sf} is the force between a sphere and a flat surface, and F_{ss} is the force between two spheres, which is the geometry used in the MASIF experiments (see below). The Derjaguin approximation is valid provided the radius of the surfaces is much larger than the distance between them. This is the case in both the SFA and the MASIF. A second requirement is that the surfaces should not deform because of the action of the surface forces. In fact, surface deformation does occur at large forces, and eq 13 is not valid for the highest forces reported in this manuscript. However, this uncertainty refers to the magnitude of the interactions force, and not to the distance of separation, and thus the (compressed) adsorbed layer thickness.

3.2.3. MASIF Instrument. The MASIF (measurement and analysis of surface interaction forces) instrument is built around a small stainless steel chamber, about 10 mL in volume. The top of the chamber, carrying the upper surface, is movable and sealed to the lower part of the chamber with a Teflon diaphragm. Coarse adjustment of the position of the upper surface is carried out using a translation stage equipped with a dc motor. The upper surface itself is mounted on a piezoelectric displacement transducer, allowing fine adjustment of its position with an accuracy of ±0.1 nm. The piezoelectric bimorph force sensor is inserted in a thin Teflon sheath onto which the holder for the lower surface is clamped. The main difficulty with using noninterferometric measurements of surface forces is how to measure the movement of the surfaces and how to calculate the distances. This is discussed briefly below and also in refs 22 and 23.

To obtain accurate measurements of the surface displacement, it is important to take into account hysteresis and creep in the piezoelectric actuator used for changing the surface separation. For this purpose an LVDT (linearly variable differential transformer) position sensor is mounted in parallel with the piezo tube. The sensitivity of the LVDT is calibrated using interferometry, either fringes of equal chromatic order (FECO) or Newton's rings, before the experiment. The LVDT sensor does not measure small changes (nm) in surface separation accurately. Hence, the LVDT signal is not used directly to measure the piezo expansion. Instead, a polynomial function is fitted to the curve showing the LVDT signal as a function of the voltage applied to the piezoelectric actuator. This smoothes out the scatter in the LVDT output, and the displacement of the upper surface can be calculated. For further details see refs 22 and 23.

During a force measurement, the surfaces are brought together in a continuous manner normally by applying a ramp voltage to the high-voltage amplifier controlling the piezoelectric actuator. Simultaneously, the bimorph response and the output from the LVDT position sensor are recorded. The duration of the force runs reported here were between 60 and 120 s. Data acquisition is completely computer controlled. For each force run the surfaces are brought into contact and then separated again. If the surfaces meet with a "hard wall" contact, the motion of the upper surface is directly transmitted to the bimorph. This is most often assumed when analyzing MASIF data and data using the atomic force microscopy (AFM−colloidal probe technique).[22] Under conditions when a hard wall contact is reached, i.e., the surfaces are incompressible, the sensitivity of the bimorph is easily calculated from the known displacement of the upper surface. Thus, the deflection of the lower surface is known at each instant, and the force exerted can be calculated by multiplication with the spring constant of the bimorph. This measuring procedure allows determination of forces as a function of separation from the hard wall contact with a high precision (about 0.1 nm in distance resolution). However, it is not possible to define an absolute position of the hard wall. As a result, the thickness of firmly adsorbed layers cannot be determined with this or other noninterferometric surface force techniques. It will be seen below that the common assumption that the surfaces reach a hard wall contact is not valid for the system studied here and that if this is not taken into account, erroneous conclusions about the range of short-range forces may be drawn.

To compare experimental data for different surfaces and to compare experiment and theory, one needs to know the radii of the surfaces. Here, the radii were simply measured by using a micrometer screw after the experiment. The drawback with this procedure is that the local radius at the interaction point, which is the radius that enters into the Derjaguin approximation (eq 13), may differ from the macroscopic radius. One may note that it has been argued that the local radius of the surface close to the contact position does not differ significantly from the macroscopic radius for flame-polished glass spheres such as the ones used here,[22] but clearly this point needs to be investigated further and the same assumption may not be valid for other surfaces.

3.3. Surface Preparation. The silica surfaces used in the ellipsometry measurements were prepared from polished silicon slides. These were oxidized thermally in oxygen followed by annealing and cooling in argon flow to generate an oxide layer with a thickness of about 30 nm. The slides were then cleaned in a mixture of 25% NH_4OH, 30% H_2O_2, and H_2O (1:1:5 by volume) at 80 °C for 5 min followed by cleaning in a mixture of 32% HCl, 30% H_2O_2, and H_2O (1:1:5 by volume) at 80 °C for 5 min. Methylated silica surfaces were prepared from the silica surfaces by subsequent double rinsing with water, ethanol, and trichloroethylene followed by treatment with a 0.1% (w/w) solution of $Cl_2(CH_3)_2Si$ in trichloroethylene for 90 min.[24] Finally, they were rinsed four times in trichloroethylene and ethanol. This procedure rendered the slides hydrophobic with advancing and receding contact angles of 95° and 88°, respectively. They were then kept in ethanol until use.

The mica surfaces used in the interferometric surface force apparatus were hydrophobically modified by Langmuir−Blodgett (LB) deposition of a monolayer of dimethyldioctadecylammonium ($DDOA^+$) ions. Dimethyldioctadecylammonium bromide was dissolved in a hexane:ethanol (95:5 by volume) mixture and spread dropwise on a pure water subphase. The LB deposition was performed with a deposition rate of 5 mm/min at a constant surface pressure (Π) of 25 mN/m (where the molecular area of $DDOA^+$ on the water phase is about 0.65 nm^2) utilizing a computerized Langmuir trough system from KSV Chemicals. The transfer ratio of $DDOA^+$, at $\Pi = 25$ mN/m, onto the negatively charged mica surface has previously been determined to be about 1.2. This gives an area per molecule after deposition of about 0.5 nm^2.[25] The obtained $DDOA^+$-coated mica surfaces were hydrophobic with advancing and receding contact angles against water of ∼105° and ∼60°, respectively.[10]

The substrate surfaces used in the MASIF instrument were spherical glass surfaces prepared by melting the end of a glass rod in a butane−oxygen burner. The surfaces obtained in this way are, according to AFM, very smooth with a typical maximum peak-to-valley roughness of 0.4 nm over a 1 μm scan, and the forces acting between such surfaces in aqueous salt solutions behave according to DLVO theory down to very small separations (D < 1−2 nm), confirming the smoothness of the surfaces.[26] Moreover, the glass surfaces obtained are hydrophilic with a contact angle close to 0°. They can easily be reacted with chlorosilanes. The surfaces used here were reacted in the gas phase with (3,3-dimethylbutyl)dimethylchlorosilane in a sealed glass vessel at room temperature for 1 h. The surfaces were then transferred to a silane-free beaker and placed in an oven at 120 °C for 1 h. The resulting hydrophobic surfaces have an advancing contact angle just above 90° and a receding angle just below 90°.

3.4. Experimental Procedure. *3.4.1. Adsorption Measurements.* Prior to adsorption, the ellipsometry measurements require a determination of the complex refractive index of the substrate.[18] In the case of a layered substrate such as oxidized silicon a correct determination of the adsorbed layer thickness and mean refractive index requires a determination of the silicon bulk complex refractive index ($N_2 = n_2 - ik_2$) as well as of the thickness (d_1) and the refractive index (n_1) of the oxide layer. This is done by measuring the ellipsometric parameters ψ and Δ in two different media, e.g., air and water. From the two sets of ψ and Δ, values of n_2, k_2, d_1, and n_1 can be determined.[18] The methyl layer is neglected for the methylated silica surfaces. All measurements were performed by four-zone null ellipsometry in order to reduce effects of optical component imperfections.[17] After optical analysis of the bare substrate surface, the B_8E_{41} block copolymer solution was added to the cuvette and the values of ψ and Δ recorded. The adsorption was monitored in one zone, since the four-zone procedure is time-consuming and since corrections for component imperfections had already been performed. Measurements at adsorption saturation showed that the uncertainty in this procedure is less than a few percent. The maximal time resolution between two measurements is 3−4 s. Stirring was performed by a magnetic stirrer at about 300 rpm. From ψ and Δ, the mean refractive index (n_f) and average

thickness (δ_{el}) of the adsorbed layer were calculated numerically according to an optical four-layer model for the methylated silica.[17] The adsorbed amount or the mass per surface area (Γ) was then derived according to $\Gamma = \delta_{el}(n_f - n_{bulk})/(dn/dc)$, using a refractive index increment (dn/dc) of 0.133 mL/g (at 30 °C) for the diblock copolymer.[7] n_{bulk} is the refractive index of the bulk solution.

3.4.2. Surface Force Measurements. Two different experimental procedures were applied in the SFA measurements. Measurements were either carried out with a droplet (of volume of about 0.1 mL) of diblock copolymer solution between the mica surfaces (droplet experiments) or with the surfaces immersed in the diblock copolymer solution, i.e., the main chamber of the SFA was filled with the solution (about 350 mL) (full box experiments). This gave two volume-to-surface area ratios differing by a factor of about 3500, which are shown below to be an important factor because of the polydispersity of the copolymer.

At the beginning of an SFA experiment, the hydrophobized mica surfaces were brought into molecular contact in air to determine the contact position defining the distance of zero separation of the surfaces. To facilitate the spreading of the block copolymer solution on the hydrophobic surfaces used in the droplet experiments, the surfaces were equilibrated in the B_8E_{41} solution outside the chamber for 1 h to let the block copolymer molecules preadsorb. However, this did not affect the wetting behavior as seen by the high meniscus contact angle when the surfaces were withdrawn from the solution. This demonstrates that the block copolymer layer was desorbing when the surfaces were passing through the three-phase line. The surfaces, which were still hydrophobic, were mounted in the SFA, and a droplet of block copolymer solution was injected between them. These diblock copolymer solutions foam very easily, and extra caution was therefore taken not to induce air bubbles between the mica surfaces. (The use of deaerated water is another precaution to minimize bubble formation on the solid surfaces.) To prevent evaporation of the droplet, a small beaker of solution with the same copolymer concentration as in the droplet was put inside the SFA during the measurements. Owing to the curved meniscus of the droplet, a Laplace pressure exists between the surfaces. This capillary pressure does not affect the measured surface force, since it is constant during the measurements. The reason is that the change in surface separation is very small compared to the curvature of the droplet. Force−distance profiles at different contact positions were measured using this procedure at two different B_8E_{41} concentrations, 10 and 50 ppm.

Full box SFA experiments (at 50 and 200 ppm) and MASIF experiments (at 50 ppm) were conducted with the hydrophobized surfaces immersed in the diblock copolymer solution. All measurements with the three experimental techniques were performed at room temperature (22−25 °C).

4. Results

4.1. Adsorption Measurements. From time-dependent ellipsometry measurements (i.e., Γ as a function of time) the adsorbed amount at equilibrium may be derived. The adsorbed amount after several hours is depicted in Figure 3 as a function of block copolymer concentration for three different EB block copolymers: diblock, triblock, and reverse triblock. The adsorbed amounts of B_8E_{41} are also given in Table 5.

Figure 4 presents the adsorbed amount as a function of time for two B_8E_{41} concentrations, 20 and 100 ppm, and it is seen that the adsorbed amount is still increasing after 1 h but the increase is small. The decrease in the 100 ppm curve at around 2600 s indicates a weak desorption when the surface was rinsed.

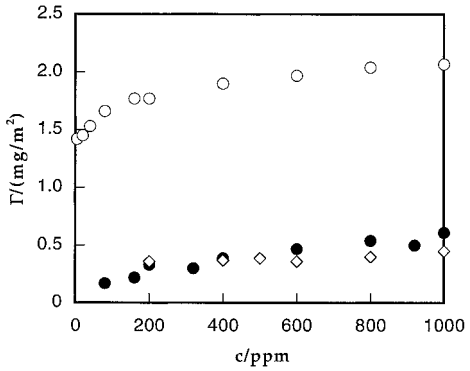

Figure 3. Adsorbed amount (Γ) as a function of block copolymer concentration (c). Adsorption isotherms obtained from ellipsometry measurements for three different EB block copolymers: B_8E_{41} (○), $E_{21}B_8E_{21}$ (●), and $B_4E_{40}B_4$ (◇).

TABLE 5: Adsorption Characteristics Obtained from Ellipsometry Measurements on the B_8E_{41}/Water System

c/ppm	Γ/(mg/m^2)[a]	Σ/nm[b]	σ/σ_{ol}[d]
5	1.42	1.98	3.30
20	1.45	1.96	3.37
40	1.53	1.91	3.55
50[e]	1.56	1.89	3.62
80	1.66	1.83	3.85
160	1.77	1.78	4.11
200	1.77	1.78	4.11
	0.43[c]	3.60	1.00

[a] Γ is here the adsorbed amount after several hours. [b] Obtained using $\pi(\Sigma/2)^2 = M_m/(\Gamma N_A)$, where $M_m = 2640$ g/mol and N_A are the weight average molecular weight of B_8E_{41} and the Avogadro constant, respectively. [c] The adsorbed amount corresponding to an average spacing of twice the radius of gyration of the poly(ethylene oxide) block ($R_g = 1.8$ nm). Below $2R_g = 3.6$ nm the interaction between the poly(ethylene oxide) chains of the adsorbed copolymer is considered to be low.[34−36] [d] Obtained using $\sigma = \Gamma N_A/M_m$ and $\sigma_{ol} = 1/(\pi R_g^2)$. The ratio $\sigma/\sigma_{ol} > 1$ indicates a stretched structure. [e] Interpolated values.

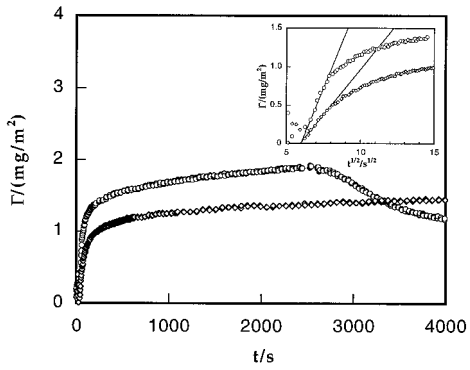

Figure 4. Adsorbed amount (Γ) as a function of time (t) for a 20 (◇) and a 100 (○) ppm solution of B_8E_{41} in water. The inset shows the adsorbed amount per unit area for 20 and 100 ppm as a function of the square root of time. The lines are linear least-squares fits of Γ versus $t^{1/2}$ for $t^{1/2} < 8.1$ s$^{1/2}$ and $t^{1/2} < 4.8$ s$^{1/2}$, respectively.

It may be noted that two adsorption regimes exist; the first is characterized by a rapid change in Γ with time. When the adsorbed amount as a function of $t^{1/2}$ is represented, as in the inset of Figure 4, the two regions are better displayed. It can be noted that the first regime is essentially linear in $t^{1/2}$ for both 20 and 100 ppm**.** The adsorbed amount at the transition from the linear to the nonlinear regime is 0.51 mg/m^2 at 20 ppm and 0.88 mg/m^2 at 100 ppm.

4.2. SFA Measurements. During an SFA measurement, each of the two hydrophobized mica surfaces will carry an adsorbed layer of B_8E_{41}. Figure 5a shows the surface forces measured between two hydrophobized mica surfaces across a 50 and a 200 ppm solution of B_8E_{41} in water, respectively, as

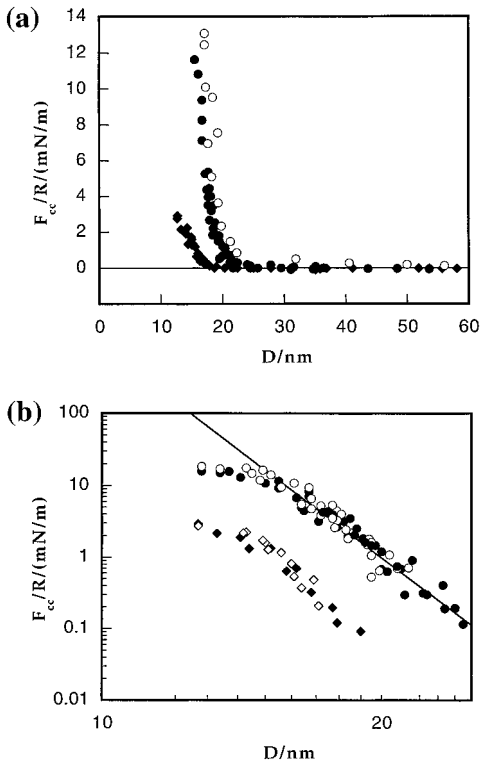

Figure 5. (a) Measured force normalized by the radius (F_{cc}/R) as a function of surface separation (D) between hydrophobized mica surfaces carrying an adsorbed layer of the diblock copolymer B_8E_{41}. The forces measured with the SFA filled with a B_8E_{41} solution are represented by ● (c = 50 ppm, separate experiments) and ○ (c = 200 ppm) and the force measured with a droplet of a 50 ppm B_8E_{41} solution by ◆. (b) Force−distance profiles of part a for a 50 ppm solution of B_8E_{41} in water shown in a double-logarithmic representation at two different volume-to-surface area ratios. ◆ and ◇ represent a droplet experiment and ● and ○ represent two different full box experiments. The filled and unfilled symbols correspond to the force measured on approach and on separation, respectively. No hysteresis exists. The line is a power law fit for D > 17.7 nm for the full box experiments.

a function of surface separation. The force−distance profiles are nearly identical, demonstrating that the adsorbed amount is nearly the same in both cases. This is in agreement with the ellipsometry measurements (see the adsorption isotherm of B_8E_{41} in Figure 3).

The 50 ppm solution of B_8E_{41} in water was investigated at two volume-to-surface area ratios differing from each other by a factor of about 3500 (full box and droplet experiment). The force profiles measured for these two cases are both shown in Figure 5a, and Figure 5b presents similar surface force data in a double-logarithmic representation. The onset of interaction ($F_{cc}/R \approx 0.1$ mN/m) is about 25 nm for the full box experiment and about 20 nm for the droplet experiment. The unperturbed (uncompressed) adsorbed layer thickness, calculated from half the distance where the onset of interaction occurs is therefore ca. 12 and 10 nm, respectively. As will be shown below, the difference in the compressed adsorbed layer thickness (the distance between surfaces at which the force has its maximum measured value) may be a consequence of polydispersity in the block copolymer sample. Figure 5b shows that for the full box measurement a power law with an exponent of −9.7 is prevalent over a large force range. No hysteresis between inward and outward force curves are observed, demonstrating that the measurements were carried out under (quasi)equilibrium conditions.

Figure 6 depicts the resulting surface force, measured in two separate droplet experiments, between hydrophobized mica surfaces across a 10 ppm B_8E_{41} solution. The onset of

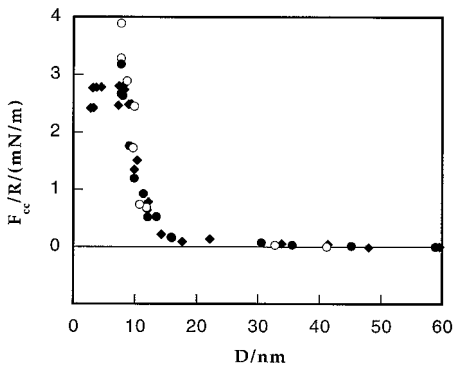

Figure 6. Force normalized by the local mean radius (F_{cc}/R), measured in two separate droplet experiment, between hydrophobized mica surfaces across a 10 ppm solution of B_8E_{41} in water as a function of surface separation (D). The filled and unfilled symbols correspond to the force measured on approach and on separation, respectively.

interaction occurs at a distance similar to that for the droplet measurement on the 50 ppm solution (Figure 5a). The measurement also demonstrates that the adsorbed layer of B_8E_{41} is more compressible at 10 ppm than at 50 ppm, and thus, it becomes thinner under a high compressive force. This may be due to a strong depletion of polymers in the droplet, leading to a lower adsorbed amount at 10 than at 50 ppm. At sufficiently high compression, an attractive force pulls the surfaces inward to adhesive contact at a distance of about 3 nm (which may be compared to $2R_g$ (=3.6 nm)[34−36] of the poly(ethylene oxide) chain). Let us first consider the forces measured on approach. When the surfaces are pressed together, the molecules will be able to move along the surface, and at a critical compressive force the two layers suddenly merge and the surfaces "jump" inward. When the force needed to induce the merging of the layers is measured a second time, immediately after the first force curve had been determined, it is shown that the force needed in order to merge the layers again is reduced. This demonstrates that it takes a considerable time before the copolymer layers have regained their initial structure. The forces measured when separating the surfaces depend on how close these are when the separation process is initiated. When the surfaces are separated before the polymer layers had been forced to merge, the same forces are observed on approach and on separation. On the other hand, when the surfaces are separated after the inward jump, a strong attractive force was experienced. The magnitude of the pull-off force at D = 3 nm varied strongly, and values between 30 and 150 mN/m were found. As a comparison, the adhesion between $DDOA^+$-coated mica without any adsorbed block copolymer is about 400−500 mN/m.

Surface force measurements performed after a 3000-fold dilution with pure water of a droplet of the 50 ppm B_8E_{41} solution show that under a high compressive force the adsorbed B_8E_{41} layer is squeezed out from between the surfaces. These force distance profiles are illustrated in Figure 7. The inset present the same data in a double-logarithmic representation, where the linear part of the diagram has a slope of −6.1. This may be compared with the slope of −9.7 for the 50 ppm concentration (Figure 5b). Clearly, desorption occurs upon dilution, which results in a less repulsive surface force and a more compressible layer.

In some cases it was observed that vibrations caused by the synchronous motor induced the formation of air bubbles stabilized by the block copolymer. When such bubbles were formed the surfaces moved outward (Figure 8). On a subsequent approach the force was considerably more repulsive compared to that before bubble nucleation had taken place (data not shown). Clearly, the forces measured in the presence of block

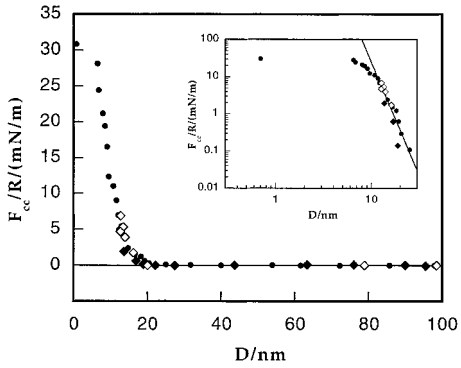

Figure 7. Force normalized by the radius (F_{cc}/R) (measured after a 3000-fold dilution with pure water of a droplet of a 50 ppm B_8E_{41} solution) between hydrophobized mica surfaces as a function of surface separation (D) under two different compression forces. At high compression force (●) the adsorbed layer is squeezed out. The filled and unfilled symbols correspond to the force measured on approach and on separation, respectively. The inset shows the force−distance profiles in a double-logarithmic representation where the line is a power law fit for $D > 12.1$ nm.

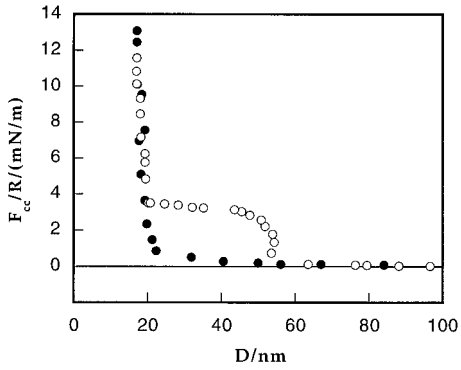

Figure 8. Force normalized by the radius (F_{cc}/R) as a function of surface separation (D) measured with the SFA filled with a 200 ppm solution of B_8E_{41} in water. Comparison between the force measured on approach (●) and on separation (○) reveals a hysteresis due to air-bubble formation.

copolymer-stabilized bubbles do not contain any information about the polymer−polymer interaction but rather reflect the force needed to deform the bubble.

4.3. MASIF Measurements. The forces measured between silanated surfaces across a 10^{-4} M KBr solution containing 50 ppm B_8E_{41} are illustrated in Figure 9. The long-range interaction is dominated by an electrostatic double-layer force. The magnitude of this interaction is similar to that observed before adding the block copolymer, and it is concluded that it originates from residual negative charges on the silanated glass surfaces. The repulsive force increases sharply when the surface separation decreases below about 2−4 nm from the hard wall contact defining $D = 0$. (The assumption of a hard wall contact will be discussed further below.) This repulsion is steric in origin as discussed above. The same forces are measured on approach and on separation over the whole force−distance curve. This demonstrates that the measurements were carried out slowly enough to allow us to ignore hydrodynamic forces and that the measurements are carried out under (quasi)equilibrium conditions.

As expected, the range of the repulsive double-layer force decreases as the salt concentration is increased (Figure 10). The magnitude of the surface potential at large separations, deduced by fitting forces calculated in the nonlinear Poisson−Boltzmann approximation to the measured forces, is rather similar in 10^{-4} M (30 mV) and in 10^{-3} M KBr (33 mV). Note, however, that this means that the surface charge density increases with increasing salt concentration. The corresponding area per charge

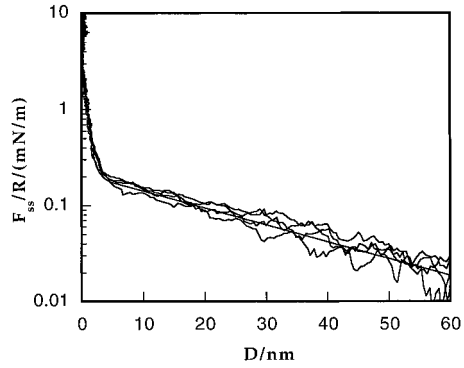

Figure 9. Force normalized by the radius (F_{ss}/R) on a logarithmic scale as a function of separation (D) between two spherical silanated glass surfaces across a 10^{-4} M KBr solution also containing 50 ppm B_8E_{41} in the MASIF. Two force curves measured on approach and two measured on separation are shown. The straight solid line represents the calculated double-layer force assuming interaction at constant charge. The Debye length used, 30 nm, corresponds to the known ionic strength. The magnitude of the surface potential at large separations was assumed to be 30 mV. The experimental data were analyzed assuming a hard wall contact at high forces.

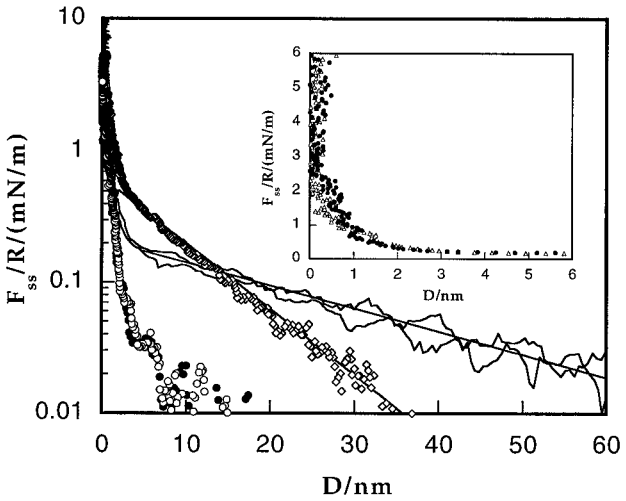

Figure 10. Force normalized by the radius (F_{ss}/R) on a logarithmic scale as a function of separation (D) between two spherical silanated glass surfaces across a solution containing 50 ppm B_8E_{41} in the MASIF. The KBr concentrations were 10^{-4} (−), 10^{-3} (◇), and 0.1 M (●, ○). The double-layer parameters used for calculating double-layer forces are in 10^{-4} M KBr, Debye length of 30 nm and a surface potential of 30 mV, and in 10^{-3} M KBr, Debye length of 9.6 nm and a surface potential of 33 mV. The inset shows the short-range forces in 10^{-4} (△) and 0.1 (●) M KBr on a linear force scale. The experimental data were analyzed using the hard wall model.

is 210 nm^2 in 10^{-4} M and 61 nm^2 in 10^{-3} M KBr. A further increase in salt concentration to 0.1 M KBr results in a complete depression of the double-layer force. A weak steric force, which increases strongly in magnitude with decreasing separation, extends out to about $D = 8$ nm. A comparison of the short-range interaction observed in 10^{-4} and 0.1 M KBr is provided in the inset of Figure 10. Clearly, the difference in interaction observed at the two salt concentrations are minor and largely due to the double-layer force present in 10^{-4} M KBr. Hence, it may be concluded that the presence of KBr up to a bulk concentration of 0.1 M does not affect the interaction between ethylene oxide segments. This is also as expected, considering that the cloud point of poly(ethylene oxide) hardly is affected by this amount of KBr.[27]

4.4. Results from Model Calculations. *4.4.1. Adsorption Isotherms.* Calculated adsorption isotherms of the three block copolymers with the same overall composition but with different architectures are shown in Figure 11. Results for both

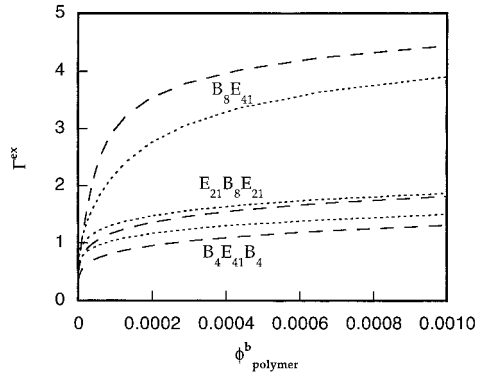

Figure 11. Calculated excess adsorbed amount (Γ^{ex}) as a function of bulk polymer volume fraction ($\phi^b_{polymer}$) for B_8E_{41}, $E_{21}B_8E_{21}$, and $B_4E_{40}B_4$ using the mass polydisperse model with interaction parameters according to Table 3 (dashed curves) and the monodisperse model with interaction parameters according to Table 4 (dotted curves).

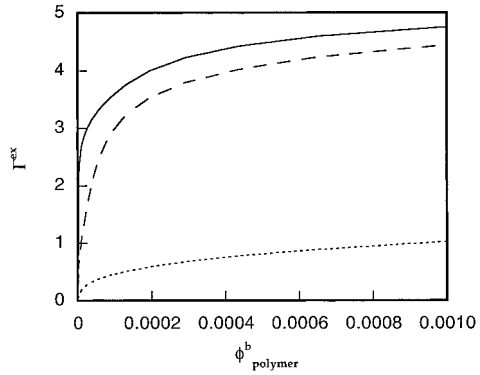

Figure 12. Calculated excess adsorbed amount (Γ^{ex}) as a function of bulk polymer volume fraction ($\phi^b_{polymer}$) for B_8E_{41} using the mass polydisperse model (dashed curve), the mass-and-composition polydisperse model (solid curve), and the monodisperse model (dotted curve), all with interaction parameters according to Table 3.

the monodisperse and the mass polydisperse models with their fitted interaction parameters are given. The theoretically calculated isotherms show that of the copolymers the diblock copolymer adsorbs most extensively, whereas the adsorption of the two triblock copolymers is similar but with a slightly more pronounced adsorption for the one having the adsorbing B block in the middle of the chain. Figure 11 also shows that given similar plateau values, polydispersity makes the isotherms of the diblock copolymer more of the high affinity type, whereas the *opposite* occurs for the triblock copolymers. It seems that the adsorption of diblock copolymer is more sensitive to polydispersity effects than the triblock copolymers. This shift makes the gap between the plateau values of the diblock copolymer and of the triblock copolymers larger as the polymers become polydisperse.

In Figure 12, the adsorption isotherms for the monodisperse model and the two representations of the polydisperse model for B_8E_{41} are shown using the *same* interaction parameters for all the calculations. Notable is the very strong increase of the adsorbed amount when only a moderate polydispersity of $M_m/M_n = 1.1$ is introduced; the plateau value increases by more than a factor of 4. Figure 12 also shows that the plateau values for the mass polydisperse and mass-and-composition polydisperse cases are similar, as already mentioned in the Model Calculations section. However, the initial rise for the second case is much steeper. Finally, as the number of components representing the mass polydisperse distribution is increased above 5 for a fixed polydispersity ratio, the adsorbed amount increases further. Since an increase in N_p makes the longest component even longer, it indicates that the longest component plays a dominant role in the adsorption.

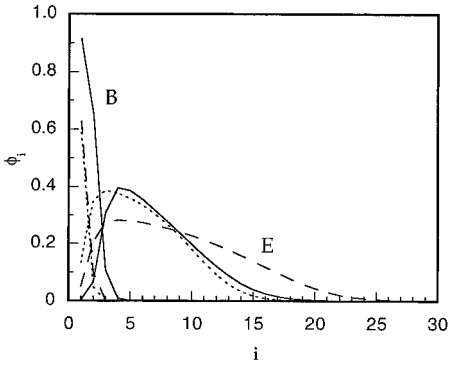

Figure 13. Calculated volume fraction of E and B segments ($\phi_{E,i}$ and $\phi_{B,i}$) as a function of layer number (i) at $\phi^b_{polymer} = 0.001$ for B_8E_{41} using the mass polydisperse model (dashed curves) and the mass-and-composition polydisperse model (solid curves) with interaction parameters according to Table 3 and the monodisperse model with interaction parameters according to Table 4 (dotted curves).

4.4.2. Volume Fraction Profiles. The volume fractions of the E and B segments perpendicular to the surface are directly obtained from the calculations according to eq 9. In Figure 13, the profiles for the E and B segments are shown for B_8E_{41} using the two polydisperse representations at a bulk volume fraction $\phi^b_{polymer} = 0.001$. As expected from the interaction parameters, the B blocks are adsorbed at the surface, whereas the E blocks are predominantly located in the outer part of the adsorbed layer. The B segments are strongly adsorbed and confined to the first two to three layers. The E blocks are strongly stretched, and their volume fraction profile displays a slowly decaying exponential tail. The amount of adsorbed B segments is 1.69 for the mass-and-composition polydisperse case compared to 0.73 for the mass polydispersity. This excess in B segments is partly compensated by the opposite relation (3.06 and 3.70, respectively) of the E segments, making the total amount adsorbed rather similar (4.75 and 4.43, respectively). Thus, we have here indications that the different E/B ratio of the components affects their tendency for adsorption.

The volume fraction profiles of the five components for the mass polydisperse case are shown in Figure 14a. Despite the small fraction of the longest components $B_{17}E_{87}$, $w = 0.013$, this component displays the largest adsorbed amount (2.8). The adsorbed amounts of the other components are arranged in molecular-mass order, the shortest component B_4E_{20} displaying a volume fraction in the first layer only slightly above its bulk value. Figure 14a also indicates that the longest component is relatively more stretched at small distances and less stretched further away from the surface. The occupation of the region at some distance from the surface by the longest components causes a depletion of the shorter components in this region as seen from the inset.

The volume fraction profiles of the end E segment (not shown) have also been examined. The layer number where these profiles display their maxima are 3, 5, 6, 10, and 15, starting with the shortest component. Since these maxima increase faster with N_E than $(N_E)^x$, $x \approx 0.5-0.6$, this shows that the longer chains are progressively more stretched than the shorter ones, supporting the picture of the long components being stretched and the short ones probably being compressed.[28]

Some of the corresponding volume fraction profiles for the mass-and-composition polydisperse case are displayed in Figure 14b. The larger number of components makes the situation more complex. However, for constant B block length, the adsorbed amount decreases with increasing length of the E block (solid curves), and for constant E block length, the amount

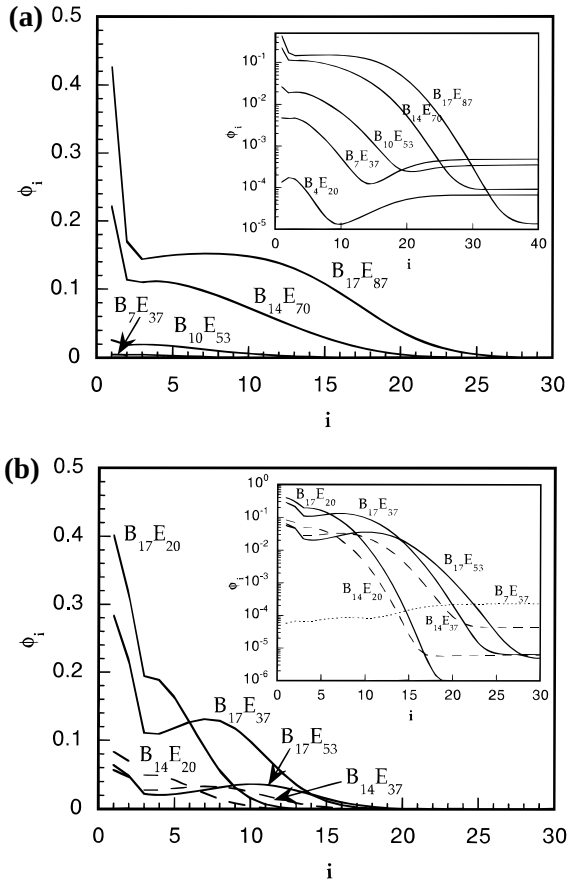

Figure 14. Volume fraction of the polymer components ($\phi_{j,i}$) as a function of layer number (i) at $\phi^{b}_{polymer} = 0.001$ for B_8E_{41} using (a) the mass polydisperse model and (b) the mass-and-composition polydisperse model with interaction parameters according to Table 3. In part b, the volume fraction of the five components with the largest volume fraction in the first layer and the component with the largest bulk volume fraction are shown. The insets show the same data on a linear−log scale.

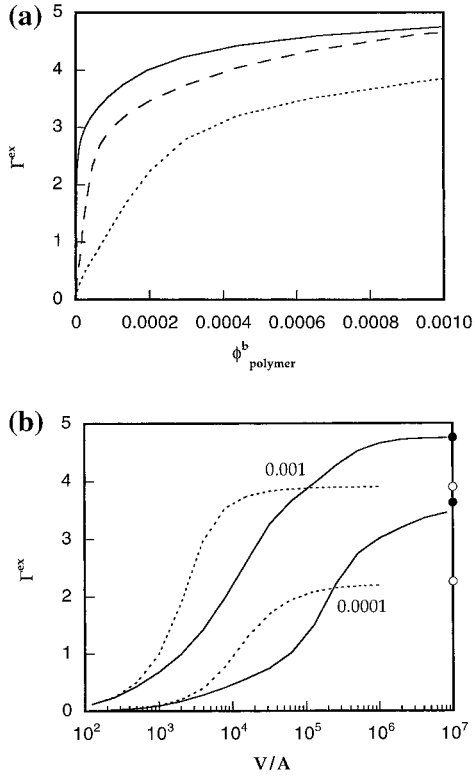

Figure 15. Excess adsorbed amount (Γ^{ex}) for B_8E_{41} as a function of (a) average polymer volume fraction ($\phi^{b}_{polymer}$) using the mass-and-composition polydisperse model at $V/A = \infty$ (solid curve), 10^6 (dashed curve), and 10^5 (dotted curve) and (b) V/A at indicated average polymer volume fraction using the mass-and-composition polydisperse model with interaction parameters according to Table 3 (solid curves) and the monodisperse model with interaction parameters according to Table 4 (dotted curves). In part b, the symbols denote the excess adsorbed amount at infinte V/A ratio.

adsorbed increases with increasing length of the B block (cf. curves for $B_{17}E_{20}$ and $B_{14}E_{20}$). The most common component in bulk, B_7E_{37}, is depleted at the surface (dotted curve). Thus, the $B_{17}E_{20}$ component shows the largest adsorbed amount, and its tendency for adsorption is so strong that, despite its fraction in bulk is only $w = 0.0002$, it constitutes one-third of the adsorbed amount (1.59). It is this difference in adsorption among the components that makes the B/E ratio of the adsorbed amount ($1.69/3.06 \approx 0.55$) almost 3 times as large as that in bulk ($8/41 \approx 0.20$).

4.4.3. Finite Volume-to-Surface Area Ratio. At low bulk concentrations and at small solution volume-to-surface area ratios (V/A), the depletion of polymers in the bulk solution due to the adsorption might be important. Figure 15a shows different adsorption isotherms at different volume-to-surface area ratios using the mass-and-composition polydisperse representation. At as large values as $V/A = 10^6$ there is already a considerable reduction of the adsorbed amount at small average polymer fractions, but at $\phi^{b}_{polymer} = 0.001$ the isotherms for an infinite system are nearly reached. At a 10-fold smaller V/A ratio, the reduction of the adsorbed amount is very pronounced in the full concentration interval displayed.

The adsorbed amount at $\phi^{b}_{polymer} = 0.0001$ and 0.001 at different V/A ratios is shown in Figure 15b. Here, corresponding data for the monodisperse model with interaction parameters giving similar plateau values of the adsorption isotherms are also given (dotted curves). As $V/A \rightarrow \infty$, the adsorbed amount approaches the values given in Figures 12 and 11, respectively, indicated by the symbols in Figure 15b. Of course, as V/A goes to zero, the adsorbed amount also goes to zero, since there are no polymers left. Taking the V/A value at which the adsorbed amount has reached half its maximum value as a measure of the influence of the finite volume, we notice that the finite volume-to-surface area effect is more important (i) at low concentrations and (ii) for polydisperse systems. For example, at $\phi^{b}_{polymer} = 0.0001$ these values are ca. 10^4 and 10^5 for the monodisperse and the mass-and-composition polydisperse cases, respectively. Thus, the value of the V/A ratio at which the adsorption is substantially reduced is strongly increased in the polydisperse case, even if the polydispersity ratio is as low as 1.1.

4.4.4. Interaction Free Energies. As mentioned in the Model Calculations section, the free energy of interaction between two surfaces immersed in a polymer solution is also directly available from the theory. Figure 16 shows this interaction free energy for the mass-and-composition polydisperse case at fixed chemical potential (equilibrium) and at fixed adsorbed amount of polymer. The amount used corresponds to the equilibrium adsorption at $M = 60$. The interaction is purely repulsive, and of course, the repulsion for the fixed amount is larger than for the equilibrium case. The inset shows that the repulsion does not fulfill a power law over the full distance range. At very low $A^{int}/(kTL)$ (below the corresponding experimental detection limit), the power becomes −17, whereas it is about −11 at $A^{int}/(kTL) = 0.01$ ($A^{int}/(kTL) = 0.01$ corresponds to the middle of the linear regime in Figure 5b).

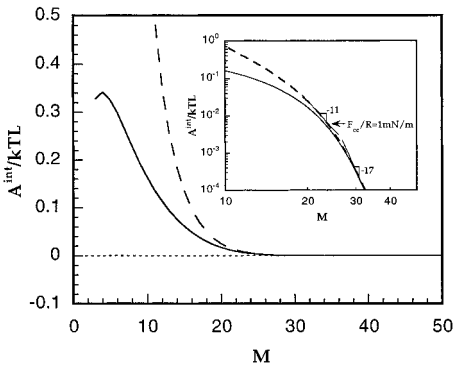

Figure 16. Interaction free energy per unit area ($A^{int}/(kTL)$) as a function of the separation (M) between the surfaces at equilibrium $\phi^{b}_{polymer} = 0.0001$ (solid curve) and at fixed polymer conditions (dashed curve) for B_8E_{41} using a mass-and-composition polydisperse model with interaction parameters according to Table 3. The inset shows the same data in a double-logarithmic representation.

5. Discussion

5.1. Adsorption Isotherms. Figure 3 illustrates the adsorption isotherms of the three different types of block copolymers, B_8E_{41}, $E_{21}B_8E_{21}$, and $B_4E_{40}B_4$, obtained from ellipsometry measurements. Since the methylated silica surface is hydrophobic, the hydrophobic B block is expected to be the adsorbing block because of the hydrophobic interaction between the block copolymer and the surface. From the adsorption isotherms it is clear that the diblock copolymer, B_8E_{41}, adsorbs the most to the hydrophobic surface. This is due to the fact that for geometrical reasons the diblock copolymers are able to pack more efficiently at the surface than any of the triblock copolymers.

The corresponding model adsorption isotherms are collected in Figure 11 for both the monodisperse and the mass polydisperse case. These results were obtained with the assumptions that (i) the interaction parameters were selected such that similar adsorption isotherms were obtained (cf. Figures 3 and 11 and remember $\Gamma/(mg/m^2) = 0.52\Gamma^{ex}$), (ii) the B segments are less soluble and more surface active that the E segments, and (iii) the polydispersity ratio $M_m/M_n = 1.1$ is taken from experimental data.

It is clear that the model is able to predict a strong adsorption of the diblock copolymer and that the adsorption of the two different triblock copolymers is smaller and similar. However, the isotherms for $E_{21}B_8E_{21}$ and $B_4E_{40}B_4$ are more separated in the calculations than in the experiments. Nevertheless, it is known that at higher concentration than used here $E_{21}B_8E_{21}$ and $B_4E_{40}B_4$ display a different tendency to form micelles,[7] and from those results it is not unreasonable to expect different adsorption behavior.

The experimental isotherms resemble more the calculated mass polydisperse isotherms in shape, with a steep initial increase in the adsorbed amount of EB and with a less steep initial rise of EBE and BEB compared to the monodisperse isotherms of the model calculations. Moreover, the increased gap between the diblock and triblock copolymers is in better agreement with the experimental data. The experimental data for B_8E_{41} are even better matched by the mass-and-composition polydispersity model, which may be seen when comparing Figure 3 with Figure 12. No calculations with mass-and-composition polydispersity were performed with the triblock copolymers because of the large number of components.

5.2. Structure of the Adsorbed Layer. The experimental and theoretical results presented provide information on the structure of the adsorbed block copolymer layer at solid surfaces. It is obvious that the B block of B_8E_{41} is the adsorbing nonsoluble anchor block while the E block is the solvated buoy block protruding into the solution. (Water is a selective solvent for the block copolymer, but no micelles are formed in the solution, since the bulk concentration is below the critical micelle concentration.) Polymers that are attached by one end to an interface (here solid−liquid, but it could also be a vapor−liquid or liquid−liquid interface) at relatively high coverage will stretch away from the interface, to avoid overlapping due to the soluble blocks' affinity for the solvent, to form a brushlike structure. This is confirmed by the mean-field calculations presented here. Generally, polymers are stretched when the average distance between adsorbed polymer chains becomes smaller than the unperturbed dimensions so that the chains begin to overlap on the surface. There are several models for describing the structure of polymer brushes (e.g., refs 2 and 3). The scaling model of Alexander-de Gennes[29−31] is based on a simple free energy balance argument from which the adsorbed amount and layer thickness, or brush height, may be derived. Experimental indications for whether the adsorbed B_8E_{41} layer has a brushlike structure or not may be obtained from the ellipsometric data that are summarized in Table 5 (and from the SFA measurements discussed below). Following the same procedure as in ref 32, the adsorbed mass per unit area at different B_8E_{41} concentrations may be used to calculate the average space between chains, Σ, from $\pi(\Sigma/2)^2 = M_m/(\Gamma N_A)$, where $M_m = 2640$ g/mol is the mass-averaged molecular weight and N_A the Avogadro number. The adsorbed mass per unit area may also be represented in terms of a surface density σ ($\sigma = \Gamma N_A/M_m$).

The surface density above which the E blocks are overlapping to form a semidilute solution in the adsorbed layer is given by $\sigma_{ol} = 1/(\pi R_g^2)$,[33] where R_g represents the radius of gyration of the E blocks in water solution. Using $R_g = 1.8$ nm for a poly(ethylene oxide) homopolymer with 41 monomer units with $M_m = 2000$ g/mol[34−36] gives $\sigma_{ol} = 0.982 \times 10^{17}$ m^{-2}. A ratio between surface densities $\sigma/\sigma_{ol} > 1$ implies that the diblock copolymers adsorb on the surface with an average distance between poly(ethylene oxide) chains that is less than the average extension of the same molecule in solution. Table 5 shows that $\sigma/\sigma_{ol} \approx 3-4$ at all concentrations at which the ellipsometry measurements were carried out. Hence, the E blocks in a coiled conformation would overlap with each other in the adsorbed layer, and the B_8E_{41} block copolymers adsorbed on the surface form a brushlike structure, or are at least somewhat stretched.

From the time-dependent ellipsometry measurements, the different processes that control the adsorption of the block copolymer molecules to a solid surface at low and high surface coverage may be discussed in a qualitative manner. In the linear regime seen at short times (Figure 4), the formation of the adsorbed layer is suggested to be controlled by diffusional transport of material to the solid surface. Thus, the time of adsorption is limited by how fast the molecules can diffuse to the surface through the stagnant layer, and this regime may therefore be referred to as the diffusion-controlled regime. The increase in the adsorbed amount with time then depends on the diffusion coefficient of the block copolymer molecules and the thickness of the stagnant layer.[37]

The diffusion- or transport-controlled increase in adsorbed amount will continue until all empty areas on the surface have been filled up. Thus, at low coverage the copolymers adsorb on the surface and are, on average, widely enough separated so that their conformation is relatively unperturbed from their conformation as free chains in solution. In the interpretation of Alexander,[29] the surface structure is said to be "mushroom-like". The deviation from linearity may then define the end of the transport-controlled regime, and beyond this transition the

increase in surface coverage is less rapid because of the interactions between block copolymer molecules at the surface, and finally, a saturation value is reached.

The adsorbed amount at the transition from the linear transport-controlled regime to the nonlinear brush regime for the B_8E_{41} concentrations 20 and 100 ppm can be used to calculate the average spacing in the same way as was made from the equilibrium adsorption values in Table 5. The values obtained from the inserted diagram of Figure 4 are 0.51 and 0.88 mg/m^2 at 20 and 100 ppm, respectively. These adsorbed amounts correspond to an average distance between the block copolymer molecules of 3.3 and 2.5 nm, to be compared to the diameter of the poly(ethylene oxide) chain of $2R_g = 3.6$ nm. Thus, there is relatively little interaction between the copolymers at the surface below the transition. The copolymers are therefore adsorbed like unperturbed single coils on the surface in the transport-controlled regime.

The force−distance profiles from SFA and MASIF measurements show a monotonic steric repulsion on compression, as expected for terminally anchored adsorbed layers in a good solvent (water is a good solvent for poly(ethylene oxide) and a nonsolvent for poly(butylene oxide)). This repulsion is caused by an increased segment density between the surfaces and a corresponding decrease in conformational entropy of the chains. At both 50 and 200 ppm an unperturbed adsorbed layer thicknesses of 12 nm is obtained from the onset of the interaction (Figure 5a). This thickness is much larger than the radius of gyration for the poly(ethylene oxide) chains ($R_g = 1.8$ nm). The thickness is in fact close to the length of a poly(ethylene oxide) chain of 41 E units in a zigzag (16 nm) or a helical (12 nm) conformation.[38] If it is assumed that the thickness of the poly(butylene oxide) region is ca. 1 nm, the E blocks on the surface must therefore be highly stretched. However, it is difficult to envision a regular and crystal-like structure in the adsorbed layer. It may also be noticed in Figure 5a that the adsorbed layer is more or less close packed already at 50 ppm, since the adsorbed layer thickness does not increase when increasing the concentration to 200 ppm, in agreement with the similar adsorbed amount obtained from the ellipsometry measurements.

The picture of the adsorbed state of the diblock copolymer is furthermore corroborated by the mean-field lattice calculations. From the calculated volume fraction profiles, it is directly seen that the poly(butylene oxide) block is the adsorbing anchor block confined to short distances away from the surface (Figure 13). The nonadsorbing E block is stretched far out in a slowly decaying feature of the density profile in a accordance with the concept of a "parabolic brush"[2,39,40] and not in the way of a step function as for the Alexander-de Gennes brush. This picture is observed for both polydisperse cases, although in the mass polydisperse case the adsorbed layer is more extended compared with the mass-and-composition polydisperse case. However, the general prediction is that the diblock copolymers are adsorbed in a brushlike structure, as was concluded from the adsorption and surface force measurements.

A calculated unperturbed adsorbed layer thickness can also be extracted from the calculated interaction energy curves at $\phi^b_{polymer} = 0.0001$ (Figure 16). By use of $A^{int}/(kTL) = 0.0006$, which corresponds to $F_{cc}/R \approx 0.1$ mN/m, a thickness of ca. 14 layers, corresponding to ca. 6 nm, is obtained. This is smaller than that deduced from the SFA measurements (12 nm). However, the corresponding thickness from the force profiles of the mass polydisperse case (not shown) is 9 nm, which is closer to the experimental data. Thus, the unperturbed adsorbed layer thickness deduced from SFA measurements and the calculations display a discrepancy. The experimental one appears to be too large for a E chain in solution. On the other hand, from the inspection of the calculated volume fraction profiles for two surfaces, these profiles have to overlap considerably before $A^{int}/(kTL) = 0.0006$ is reached [can also be inferred from Figure 13, where the data is for $\phi^b_{polymer} = 0.001$ but the volume fraction profiles are not changed very much for $\phi^b_{polymer} = 0.0001$)]. Obviously, the model with the selected interaction parameters and polydispersity ratio is not capable of representing accurately the repulsive force of the two approaching surfaces. A possible reason may be that the real sample contains a few molecules that are significantly longer than the average one. The tails of these molecules may dominate the most long-range part of the interaction. Another explanation could be that the onset of the force is relatively sensitive on the mapping of the nonspherical ethylene oxide monomer on a spherical segment.

5.3. Effect of Polydispersity. An often detected feature in surface tension measurements of di- and triblock copolymers is the absence of any break in the surface tension versus copolymer concentration curve.[7] A minimum of the surface tension is sometimes observed in the vicinity of the change in slope of the curve, which is attributed to hydrophobic components[5] (see also ref 1 and the references therein). In the surface tension measurements performed recently using the de Nouy ring method (not shown) on B_8E_{41}, a decrease in surface tension with time was observed at low copolymer concentrations. This indicates a polydisperse system in which more hydrophobic species exist that adsorb slowly onto the air−water interface.[41]

The time-dependent ellipsometry measurements illustrated that the time needed to reach adsorption equilibrium is rather long, again indicating a polydispersity of the diblock copolymer. It is expected that different components will dominate the adsorption at different times. The shorter chains will adsorb first because of a faster diffusion to the surface. These will then slowly be replaced by larger and more hydrophobic components until an equilibrium as depicted by the mean-field calculations is reached. These calculations show that the adsorption increases strongly with increasing length of the B block and increases less strongly with reducing length of the E block. The adsorption isotherms obtained from the model calculations also demonstrated that the isotherm of B_8E_{41} shifts to a more high affinity type when polydispersity is introduced as a variable (see Figure 11). The effect is even more pronounced in the mass-and-composition polydispersity case of B_8E_{41} (Figure 12).

When the volume-to-surface area ratio was varied in the SFA measurements, a clear shift in the adsorbed layer thickness to a larger value was observed with a higher volume-to-surface area ratio (Figure 5a). For a monodisperse polymer sample such a behavior is to be expected when the surface has not been fully saturated of polymers because of the small solution volume available. For a polydisperse sample such a shift is expected to occur even at much larger volume-to-surface area ratios. The reason is that at a finite volume-to-surface area ratio, the largest and most hydrophobic components are not present in sufficient quantities to cover the surface to the same degree as when a large volume of solution is in contact with the surface. Hence, these components are depleted from the solution, and the adsorbed amount, the extension of the polymer layer, and the range of the steric forces all decrease with decreasing volume-to-surface area ratio.

The conditions of the drop experiment at 50 ppm correspond to an amount of polymer ca. 10 times the adsorbed amount given in Figure 3. Thus, the inward shift of the force profile for the drop experiment in Figure 5a is not consistent with a monodisperse sample. Moreover, using $d = 0.4$ nm, one gets $V/A \approx 10^6$ (in reduced units), and Figure 15b confirms that the surface

is saturated with polymer at $\phi^{b}_{polymer} = 0.0001$ (100 ppm) at that V/A ratio. However, the same figure also shows that for a polydisperse polymer model the adsorbed amount is reduced by ca. 20% compared with $V/A = \infty$, and this reduction is increased with decreasing concentration. Thus, one may conclude that the different volumes in the full box and drop experiments in combination with a polydisperse sample contribute to the different force curves observed.

The volume fraction profiles obtained from the model calculations of the five components for the mass polydisperse case show that the longest component is relatively more stretched than the shorter components in the region adjacent to the solid surface (Figure 14a). Further away from the surface the longest component is less stretched. This result is in line with a theoretical study of the effect of polydispersity on the polymer brush, using a numerical self-consistent-field model.[28] A bimodal molecular weight distribution was used in that study as a model system for polydispersity. The longer chains were found to be stretched through the inner region at small distances from the surface, and the longer chain ends were found to be localized at the outer edge of the polydisperse polymer brush.

Recently, surface force measurements of the interactions between adsorbed layers of a diblock (and triblock) copolymer of polystyrene and poly(vinylpyridine) in toluene have been conducted in order to investigate the effects of polydispersity on polymer brushes.[42] The layers were obtained by mixing different lengths for the nonadsorbing block. It was found that the force−distance profiles for a bimodal distribution deviated from the profile of a monodisperse sample in the low-compression limit. This was explained as a manifestation of the fact that the density profiles in the outer region of the layers with the bimodal distribution differ from that in the layer of the monodisperse sample, as discussed above.

5.4. Surface Force Profiles. Equation 13 infers that the force measured with the SFA or the MASIF is related to the free energy of interaction per unit surface area between two flat surfaces covered with B_8E_{41}. This interaction free energy per unit area is also obtainable from theory ($A^{int}/(kTL)$). Figure 16 displays $A^{int}/(kTL)$ for the mass-and-composition polydisperse case at equilibrium and at fixed amount of block copolymer as a function of number of lattice layers. The experimental force−distance profiles are given in Figure 5a. By direct comparison between them it is noticed that all curves are purely repulsive but the force of the experimental curves begins at larger separations, as already discussed. The insets of Figure 16 and Figure 5b display the theoretical and the experimental curves in a double-logarithmic representation, respectively. Both curves display a concave shape. The onset of the bending at large forces appears at a lower force in the model system compared to the experimental results, and the slope at low forces is exaggerated, −17 compared to −10. However, at comparable forces ($A^{int}/(kTL) = 0.01$ and $F_{cc}/R = 1.6$ mN/m) the slopes become similar. Thus, it appears that the model system reasonably well represents the force−distance curve at intermediate and strong forces but that the force is too weak at large separations. Although the force curve calculated at fixed amount has been used in the analyses made here, it is not possible at the present stage to judge whether the fixed chemical potential or the fixed amount condition is the most appropriate one to use.

The short-range forces measured between hydrophobic silanated surfaces using the MASIF technique and the forces acting between hydrophobized mica surfaces, measured using the interferometric SFA, across a 50 ppm B_8E_{41} solution are compared in Figure 17. To facilitate this comparison, one has to take into account the difference in geometry of the interacting surfaces used (two spheres in the MASIF and two crossed cylinders in the SFA). This is easily done using the Derjaguin approximation (eq 13). Second, one has to remember that with the MASIF technique one does not obtain the absolute distance but rather the distance away from the hard wall. Hence, in Figure 17 the results obtained with the two techniques have been forced to coincide at a F_{ss}/R value of 5 mN/m, which is at the position of the hard wall inferred when analyzing the MASIF data. Clearly, the range of the steric repulsion obtained with the SFA is larger, by about 2 nm, and less steep than that obtained with the MASIF. This is rather unsatisfactory, since it is believed that the adsorption, which is driven by the hydrophobic interaction, should be very similar on the two types of hydrophobic surfaces used.

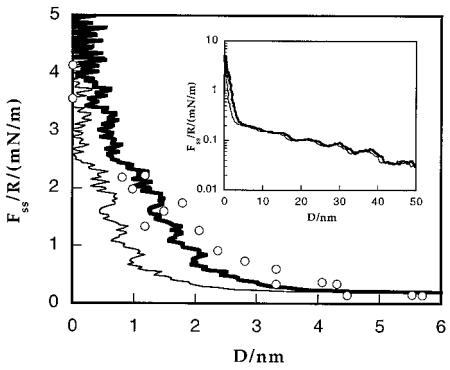

Figure 17. Force normalized by the radius (F_{ss}/R) as a function of surface separation D between hydrophobic surfaces across a 10^{-4} M KBr solution containing 50 ppm B_8E_{41}. The forces were measured using the MASIF technique and spherical silanated glass surfaces. The analysis of the data was carried out by assuming a hard wall contact (thin line) or a compressible wall contact (thick line); for details see text. The forces measured using the interferometric surface force technique and hydrophobized mica are represented by ○. These forces are converted to spherical geometry using the Derjaguin approximation. The inset shows the force normalized by the radius on a logarithmic scale as a function of separation between two spherical silanated glass surfaces across a 10^{-4} M KBr solution also containing 50 ppm B_8E_{41}.

The explanation for the discrepancy can, however, be found and seen to originate from the assumption of a hard wall contact that was made when analyzing the MASIF data. When inspecting the force curves determined with the interferometric SFA, one finds that no hard wall is reached. Instead, the adsorbed layers have a significant compressibility at the force values where it was assumed that a hard wall had been encountered in the MASIF analysis. However, the results obtained with the two techniques agree very well with each other when the MASIF data are reanalyzed using a compressible wall approximation with a compressibility determined from the force curves deduced with the interferometric SFA (Figure 17). Clearly, care should be taken when analyzing surface force data from noninterferometric techniques. In particular, the commonly made assumption of a hard wall contact may not always be correct. This is especially critical when interactions between polymer-coated surfaces are investigated.

The inset of Figure 17 illustrates how the long-range force measured with the MASIF is affected when the compressible wall approximation is used instead of the hard wall approximation. Also, in this case the force curves are shifted relative to each other. However, owing to the slowly decaying form of the force curve, this shift is unimportant and does not significantly affect the deduced decay lengths and surface potentials.

6. Conclusions

Experimental studies of block copolymers of poly(butylene oxide) and poly(ethylene oxide) at interfaces have here been

combined with lattice mean-field calculations. The interaction parameters needed in the mean-field calculations were obtained by fitting the experimentally determined adsorption isotherms for both the diblock and the two types of triblock copolymers by the theoretical calculations. Once the interaction parameters were established, the theoretical model was used to study how the structure of the adsorbed layer was dependent on polydispersity and volume-to-surface ratio. It was found that even for such a small polydispersity ratio as 1.1 the composition of the adsorbed layer was very different from that in bulk solution. It was also found that the structure of the adsorbed layer will differ if one considers either mass polydispersity only or both mass and composition polydispersity. There is a strong enrichment of high molecular weight and oxybutylene-rich polymer components at the surface. These components are not common in bulk solution, which means that at small volume-to-surface ratios they become depleted, and the volume-to-surface ratio affects the adsorbed layer. This effect was confirmed by experiments.

From surface force measurements it was found that adsorption of the B_8E_{41} block copolymer generated long-range steric forces that were the same on approach and on separation. The range of these quasi-equilibrium forces indicates the presence of extended chains. This is qualitatively expected from the calculations. However, the observed range of the steric force was somewhat larger than predicted. Finally, it is noted that care should be taken when analyzing surface force data obtained with noninterferometric techniques. Particularly, for this case with block copolymer-coated hydrophobic surfaces it was found that the common assumption of a hard wall contact was not valid.

Acknowledgment. The copolymers used in this study were synthesized by Dr. Zhuo Yang, University of Manchester. Financial support from the Swedish Research Council for Engineering Sciences (TFR) and the Engineering and Physical Science Research Council (U.K.) is gratefully acknowledged.

References and Notes

(1) (a) Alexandridis, P.; Hatton, T. A. *Colliods Surf. A* **1995**, *96*, 1. (b) Zhou, Z.-K.; Chu , B. In *Nonionic Surfactants*; Nace, V. M., Ed.; Marcel Dekker Inc.: New York, 1996; Vol. 60, Chapter 3.

(2) Fleer, G. J.; Cohen Stuart, M. A.; Scheutjens, J. M. H. M.; Cosgrove, T.; Vincent, B. *Polymers at Interfaces*; Chapman & Hall: London, 1993.

(3) Milner, S. T. *Science* **1991**, *251*, 905.

(4) Grest, G. S.; Murat, M. In *Monte Carlo and Molecular Dynamics Simulation in Polymeric Science*; Binder, K., Ed.; Oxford University Press: Oxford, 1995.

(5) Bedells, A. D.; Arafeh, R. M.; Yang, Z.; Attwood, D.; Heatly, F.; Padget, J. C.; Price, C.; Booth, C. *J. Chem. Soc., Faraday Trans.* **1993**, *89*, 1235.

(6) Tanodekaew, S.; Deng, N.-J.; Smith, S.; Yang, Y.-W.; Attwood, D.; Booth, C. *J. Phys. Chem.* **1993**, *97*, 11847.

(7) Yang, Z.; Pickard, S.; Deng, N.-J.; Barlow, R. J.; Attwood, D.; Booth, C. *Macromolecules* **1994**, *27*, 2371.

(8) Yu, G.-E.; Yang, Y.-W.; Yang, Z.; Attwood, D.; Booth, C.; Nance, V. M. *Langmuir* **1996**, *12*, 3404.

(9) Yang, Y.-W.; Deng, N.-J.; Yu, G.-E.; Zhou, Z.-K.; Attwood, D.; Booth, C. *Langmuir* **1995**, *11*, 4703.

(10) Scheutjens, J. M. H. M.; Fleer, G. J. *J. Phys. Chem.* **1979**, *83*, 1619.

(11) Scheutjens, J. M. H. M.; Fleer, G. J. *J. Phys. Chem.* **1980**, *84*, 178.

(12) Flory, P. J. *Principles of Polymer Chemistry*; Cornell University Press: Ithaca, New York, 1953.

(13) Evers, O. A.; Scheutjens, J. M. H. M. *Macromolecules* **1990**, *23*, 5221.

(14) Linse, P.; Björling, M. *Macromolecules* **1991**, *24*, 6700.

(15) Linse, P. *Macromolecules* **1994**, *27*, 6404.

(16) *Polymer Handbook*; Brandrup, J., Immergut, E. H., Eds.; Wiley: New York, 1989.

(17) Azzam, R. M. A.; Bashara, N. M. *Ellipsometry and Polarized Light*; North-Holland: Amsterdam, 1989.

(18) Landgren, M.; Jönsson, B. *J. Phys. Chem.* **1993**, *97*, 1656.

(19) Israelachvili, J. N.; Adams, G. E. *J. Chem. Soc., Faraday Trans. 1* **1978**, *74*, 975.

(20) Israelachvili, J. N. *J. Colloid Interface Sci.* **1973**, *78*, 259.

(21) Derjaguin, B. *Kolloid Z.* **1934**, *69*, 155.

(22) Parker, J. L. *Prog. Surf. Sci.* **1994**, *47*, 205.

(23) Claesson, P. M.; Ederth, T.; Bergeron, V.; Ruthland, M. W. *Adv. Colloid Interface Sci.* **1996**, *67*, 119.

(24) Jönnson, U.; Ivarsson, B.; Lundström, I.; Berghem, L. *J. Colloid Interface Sci.* **1982**, *90*, 148.

(25) Herder, P. C.; Claesson, P. M.; Herder, C. E. *J. Colloid Interface Sci.* **1987**, *119*, 155.

(26) Claesson, P. M.; Parker, J. L.; Fröberg, J. C. *J. Dispersion Sci. Technol.* **1994**, *15*, 375.

(27) Florin, E.; Kjellander, R.; Eriksson, J. C. *J. Chem. Soc., Faraday Trans. 1* **1984**, *80*, 2889.

(28) Dan, N.; Tirrell, M. *Macromolecules* **1993**, *26*, 6467.

(29) Alexander, S. *J. Phys. (Paris)* **1977**, *38*, 977.

(30) de Gennes, P. G. *Macromolecules* **1980**, *13*, 1069.

(31) de Gennes, P. G. *Adv. Colloid Interface Sci.* **1987**, *27*, 189.

(32) Amiel, C.; Sikka, M.; Schneider, J. J. W.; Tsao, Y.-H.; Tirrell, M.; Mays, J. *Macromolecules* **1995**, *28*, 3125.

(33) Tirrell, M. Solvents and Self-Organization of Polymers. Lectures presented at NATO ASI, Turkey, August, 1995.

(34) Bhat, R.; Timasheff, S. N. *Protein Sci.* **1992**, *1*, 1133.

(35) Li, J.-T.; Caldwell, K. D.; Rapoport, N. *Langmuir* **1994**, *10*, 4475.

(36) Devanand, K.; Seiser, J. C. *Macromolecules* **1991**, *24*, 5943.

(37) Kop, J. M. M.; Corsel, J. W.; Janssen, M. P.; Cuypers, P. A.; Hermens, W. T. *J. Phys.* **1983**, *C10*, 491.

(38) Craven, J. R.; Hao, Z.; Booth, C. *J. Chem. Soc., Faraday Trans.* **1991**, *87*, 1183.

(39) Milner, S. T.; Witten, T. A.; Cates, M. E. *Macromolecules* **1988**, *21*, 2610.

(40) Zhulina, E. B.; Borisov, O. V.; Priamitsyn, V. A. *J. Colloid Interface Sci.* **1990**, *137*, 495.

(41) Mysels, K. J. *Langmuir* **1986**, *2*, 423.

(42) Dhoot, S.; Watanabe, H.; Tirrell, M. *Colloids Surf. A* **1994**, *86*, 47.

(43) Yang, Y.-W.; Tandodekaew, S.; Mai, S.-M.; Booth, C.; Ryan, A. J.; Bras, W.; Viras, K. *Macromolecules* **1995**, *28*, 6029.

(44) Malmsten, M.; Linse, P.; Zhang, K.-W. *Macromolecules* **1993**, *26*, 2905.